Incorporation of Ni into HZSM-5 zeolites: Effects of zeolite morphology and incorporation procedure

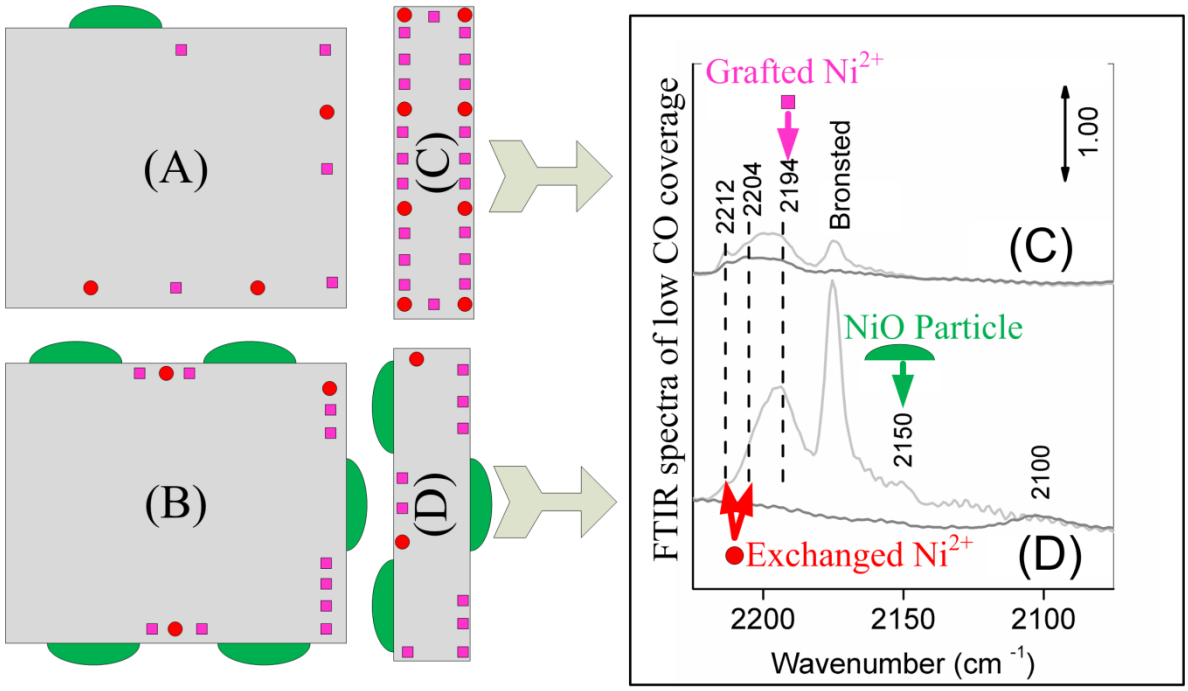

Graphical Abstract: Incorporation of nickel in ZSM-5 zeolites with different morphologies and different insertion routes: (A) Commercial Ni-ZSM-5 prepared by ion exchange, (B) Commercial Ni-ZSM-5 prepared by impregnation, (C) Nanosheet Ni-ZSM-5 prepared by ion exchange, (D) Nanosheet Ni-ZSM-5 prepared by impregnation method.

Incorporation of Ni into HZSM-5 Zeolites: Effects of zeolite morphology and incorporation procedure

Yadolah Ganjkhanlou,[1] Elena Groppo,[1] Silvia Bordiga,[1] Mariia Anatol'evna Volkova,[2] Gloria Berlier[1]*

[1] Dipartimento di Chimica, NIS Centre of Excellence and INSTM Università di Torino, Via P. Giuria 7, 10125 Turin, Italy.

[2] Ivanovo State University of Chemistry and Technology, Sheremetev av., 7, 153000, Ivanovo, Russia

Email of corresponding author: gloria.berlier@unito.it

Received date: XX/XX/2015

Abstract

Insertion of Ni species into H-ZSM5 catalysts with high Si/Al ratio (around 50) and different morphology (micron sized particles *vs* nanosheet ones) has been carried out by two different methods, namely impregnation and ion exchange routes. The resultant samples have been characterized by IR spectroscopy using CO as probe molecule after thermal treatment in oxygen or vacuum. In all samples different Ni^{2+} surface sites (counterions, grafted or on the surface of NiO particles) have been observed, but their distribution and concentration were

found to be greatly influenced by morphology of zeolite particles as well as Ni incorporation method. For instance, the nanosheet morphology was found to favour ion exchange, probably in relation to high amount of surface tetrahedral Al sites. Moreover, a small fraction of sites was found to be reduced, both to Ni^{+} counterions and Ni^{0} (nano) particles, when the activation was carried out in vacuum in some of the samples. This could be related to changes in the population of surface OH groups (Brønsted sites and hydrogen bonded silanols), and to the formation of surface defects (strained Si-O-Si bridges). These observations give indications about the mechanism governing ion reactivity and migration in zeolite matrices, and confirm the fact that silanol groups are of the utmost importance in affecting the dispersion of the metal phase, and therefore the corresponding redox properties.

Keyword: HZSM-5; Impregnation; Ion exchange; IR spectroscopy.

1-Introduction

ZSM-5 zeolite is an important heterogeneous catalyst that could be applied in different industrial processes to catalyse various petrochemical reactions as well as reduction and decomposition of greenhouse gases (for instance methanol-to-gasoline process, hydrocarbon isomerization, olefin oligomerization and reduction of NOx with hydrocarbons) [1-5]. It is a microporous aluminosilicate with MFI-framework containing tetrahedral silicon and aluminium sites where a proton is present next to the aluminium tetrahedral site to compensate the negative charge generated on framework oxygen atoms[5]. The main advantage of this catalyst is its shape-selectivity which makes it good candidate for specific

reaction such as ethylene oligomerization [2]. The shape dependent surface chemistry and catalytic performance are important characteristics of this type of catalyst, which gained even more attention in recent years due to nanotechnology development [6, 7].

Apart from the chemical composition and intrinsic porosity of a zeolite framework structure, morphology can play an important role in determining its catalytic performances. Commercial ZSM5 zeolites usually consist of micron sized particles which may cause some constraints in catalytic reactions, such as high contact time and slow rate of reaction due to diffusion limitation which could cause cocking [5]. Reduction of the particle size as well as changing the morphology are two reported methods to overcome these limitations. Recently, ZSM-5 with sheet-like morphology has been prepared by Ryoo's group [6, 7]. This sheet-like morphology may influence the contact time in catalytic reactions and therefore may an effect on products composition [8].

Modified ZSM5 zeolites with various transition metal ions showed increased activity toward specific reactions; for instance copper-exchanged ZSM-5 zeolites could be utilized for direct decomposition of NO [9]. It was also reported that Ni containing ZSM-5 zeolites have promising catalytic activity due to unique cationic sites of ZSM5 zeolite [10, 11]. Low coordination number of Ni cations in ZSM-5 structure and ability of this zeolite to stabilize Ni cations in low-valence states are the main reasons for the superior catalytic activity of Ni containing ZSM5 zeolite in comparison with other zeolites [11]. A comprehensive study by Pietrzyk et al. [12, 13] using different techniques (e.g. IR spectroscopy, EPR, HYSCORE and DFT calculations) also confirmed the suitability of Ni-ZSM5 zeolite as catalyst for some important reactions such as NO_x reduction, oxidation of CO, methanol synthesis and CO hydrogenation.

It is apparent that the oxidation and coordination state of the nickel ions in ZSM5 frameworks are decisive in its catalytic activity [12, 13], and these parameters can be affected by Ni insertion method as well as morphology of ZSM-5 zeolites. Although the different sites formed by Ni incorporation into the ZSM5 zeolite have been greatly studied by various researchers through the world [3, 4, 14], but the effects of Ni insertion method and zeolite morphology as separate parameters have never been investigated in literature. In this contribution, two different preparation procedures (impregnation and ion exchange) have been employed to add Ni species into ZSM5 zeolites with different morphologies (micron sized particle and nanosheet morphology). The resultant samples have been investigated with infrared spectroscopy coupled to the employ of probe molecules in order to shed light on the insertion mechanism of Ni counter ions (ion exchange and grafting) in the different starting materials.

2.Experimental

2.1. Materials

Two H-ZSM5 samples with similar Si/Al ratio were employed as starting materials for Ni insertion. Namely, commercially available microsized H-ZSM5 material (Zeochem International: PZ-2/100H, Si/Al = 59), which is labeled as Comm-H in the following and the home-made nanosheet H-ZSM5 sample (NS-H, Si/Al = 51), which was synthesized as described in the literature [15].

Ni was added to the samples by two different routes (impregnation and ion exchange). Impregnation was carried out by dissolving 0.5 g of nickel acetylacetonate ($[Ni(acac)_2]_3$,

where acac is the anion $C_5H_7O_2^-$) in 20 mL of toluene. 5 g of zeolite was added to the solution, stirred at room temperature (RT) for half an hour and toluene was then evaporated in a rotary evaporator. The corresponding Ni loading was 2 wt% (confirmed by EDS analysis). Next, the samples were calcined in air flow from RT to 823 K, and left at this temperature for 6 hours. Resulting samples are hereafter labelled as Comm-Ni/impr (commercial) and NS-Ni/impr (nanosheet).

Ion exchange of the two parent zeolites was carried out by employing a 0.1 M $Ni(NO_3)_2$ aqueous solution. 20 ml of this solution were employed to exchange 2 grams of zeolite with stirring at 70 °C for 2 hours. This was repeated for 5 times. The employed Ni amount was calculated in order to get the same final Ni loading as in the impregnated samples. However, the final loading was found to be too small for accurate EDS analysis (around 0.5 wt%). The samples were then calcined at 873 K as already described. Resulting samples are hereafter labelled as Comm-Ni/i.e. (commercial) and NS-Ni/i.e. A summary of the investigated samples and of the adopted nomenclature is reported in Table 1.

Table 1.Summary of the different ZSM-5 samples

		Commercial	**Nanosheet**
Protonated		Comm-H	NS-H
Nickel	Ion-exchanged	Comm-Ni/i.e.	NS-Ni/i.e.
	Impregnated	Comm-Ni/impr	NS-Ni/impr

2.1. FTIR spectroscopy

For FTIR spectroscopy of adsorbed probe molecules, all samples were pressed into self-supporting wafers and IR spectra measured in transmission mode on a Bruker IFS 66 FTIR spectrometer equipped with a mercury cadmium telluride (MCT) cryodetector working with a 2 cm^{-1} resolution.

Thin self-supporting wafers of each sample were placed inside an IR cell designed to allow *in situ* high temperature treatments, gas dosage, and low-temperature measurements. Prior to adsorption experiments samples were thermally treated in oxidant conditions or in vacuum. In the former, the samples were heated in vacuum up to 423 K, and O_2 (100 mbar) was dosed twice at this temperature, outgassing the sample for 15 minutes between the two gas dosages. The pellet was then heated in O_2 up to 673 K and left at this temperature for 1 hour. Cooling down of the sample to RT was carried out in O_2, by removing it at 423 K. Activation in vacuum was carried out by heating the sample at 673 K and leaving at this temperature for 1 hour before cooling down to RT.

CO adsorption experiments were carried out at liquid nitrogen temperature (LNT) by sending 30 Torr of CO on the zeolites and stepwise decreasing the pressure. For all samples, the spectrum before CO dosage was used as reference to obtain the subtracted spectra reported in the CO stretching region (νCO). For comparison spectra were normalized by employing the fingerprint region of silicate frameworks in the 1750–2100 cm^{-1} region.

3. Results and discussion

3.1. Influence of Ni insertion on OH population

The ν(OH) vibrational region of IR spectra of sample activated in oxidizing atmosphere are shown in Figure 1 (spectra in the whole IR region can be found in the supporting information, Figure S1). The spectrum of Comm-H sample (curve a in left panel) shows absorption bands at 3745/3726, 3700, 3613 and 3495 cm^{-1}. Most of the bands are related to silanols, as extensively described in Ref [16]. Namely: the bands at 3745 cm^{-1} was assigned to isolated silanol groups on the external surface and the bands at 3726 and 3700 cm^{-1} to silanol groups inside the zeolite crystals. The broad band at 3495 cm^{-1} was ascribed to hydroxyl nests, which consist of a number of silanol groups interacting through extended hydrogen bonding, inside the zeolite pores [16]. The typical Si(OH)Al Brønsted sites formed by the OH groups located between a Si and Al atom in the crystal structure are found at 3613 cm^{-1}. Similarly to other commercial H-ZSM-5 samples, the relative intensity of the bands assigned to Si-OH species (external, internal, free or hydrogen bonded) is comparable to that of the band due to Si(OH)Al Brønsted sites.

The IR spectrum of the NS-H sample is substantially different and dominated by the strong absorption band due to free silanols (3745 cm^{-1}), with a tail down to 3250 cm^{-1} and with weak bands at 3670 and 3613 cm^{-1}, which are related to defective extra-framework Al-OH and Brønsted sites, respectively (curve a in Figure 1, right panel). These features are related to the unique crystal structure of the nanosheets. Indeed, in this sample the growth of the crystallites along the b-axis of the framework is inhibited by structure directing agent and the crystallites grow in *a* and *c* directions of unit cell. The new crystal morphology considerably changes the ratio of the internal and external surfaces. For a cubic crystal of a commercial H-ZSM-5 with the size of 100 nm in each direction, only 2% of the tetrahedral atoms (Si or Al at vertices of pentasils) are external, while in a nanosheet crystallite with dimensions of

16*4*19 nm the estimated fraction of tetrahedral atoms on the external surface approaches 20% of the total. This morphology also affects the local structure of the Brønsted acid sites related to the framework Al^{3+} [5].

Upon addition of nickel on Comm-H zeolite by impregnation the IR spectrum substantially changes (curve b in left panel of Figure 1). The relative and overall intensity of all the bands described above decreases, indicating that the impregnation process has modified the population of both Brønsted sites (bands at 3613 cm^{-1}) and silanols. Among the latter, the most affected bands are those at 3727, 3700 and 3495 cm^{-1}, related to internal free or hydrogen bonding groups. Moreover, the broad band centred at 3495 cm^{-1} in pristine material is now blue-shifted (+ 20 cm^{-1}). Simultaneously, a new band appears at 3658 cm^{-1}, which can be tentatively assigned to Ni-OH surface groups. This could be related to Ni^{2+} sites grafted, present at the surface of NiO particles or to $[Ni\text{-}OH]^{+}$ counterions, in analogy with what observed on Cu-exchanged zeolites [17]. On the contrary, no considerable difference is noted between the IR spectra of Comm-Ni/i.e. and that of Comm-H samples (curves a and c in Figure 1, left panel).

When the spectra of nanosheet samples are considered, the situation is almost the reverse. Insertion of Ni by impregnation causes practically no changes in the IR spectrum with respect to parent material (compare spectra a and b in right panel of Figure 1). On the contrary, an evident decrease of the Brønsted band at 3613 cm^{-1}) is observed in sample NS-Ni/i.e. (curve c).

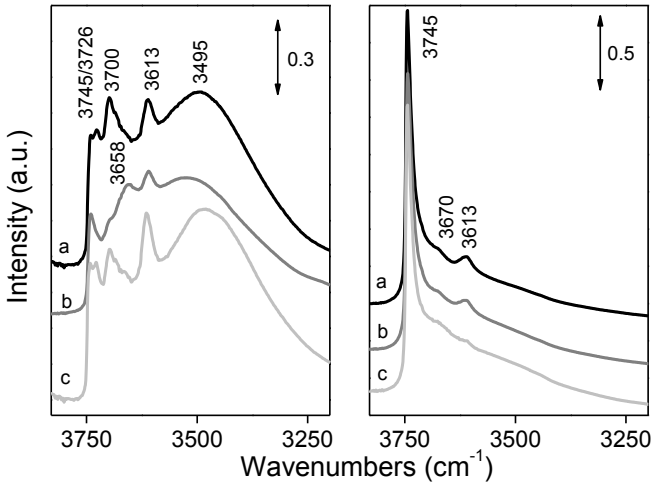

Figure1. IR spectra of oxidized sample in the νOH region. Left: a) Comm-H, b) Comm-Ni/impr and c) Comm-Ni/i.e.Right:a) NS-H, b) NS-Ni/impr and c) NS-Ni/i.e. Spectra were vertically shifted for easier comparison

The results described above suggest that different mechanisms can be drawn to describe the insertion of Ni in the present ZSM-5 samples, and that these are strongly influenced by the samples morphology. Ion exchange is expected to result in the consumption of Si(OH)Al Brønsted sites (3613 cm^{-1}) which are replaced by Ni^{2+} ions. This can be clearly observed in NS-Ni/i.e. but only in very small amount in Comm-Ni/i.e., suggesting that in nanosheet samples the probability for Ni^{2+} to exchange with Brønsted H^{+} sites increased, likely due to presence of more tetrahedral Al atoms on the external surface.

Another mechanism for Ni insertion is grafting, which can take place by reaction with internal or external silanol groups, similarly to what occurring on the surface of amorphous silica [18-21]. This is the main mechanism (together with ion exchange) taking place on sample Comm-Ni/impr, as testified by the decrease in the intensity of the (internal) silanol

bands at 3727, 3700 and 3495 cm^{-1}. Moreover, the shift of the broad band at 3495 cm^{-1} indicates a redistribution in the hydrogen bonded nests within the zeolite channels. This analysis does not give indications about the nuclearity (isolated, dimeric etc.) of grafted Ni sites and about the possibility of NiO aggregates formation on the external surface of the zeolites. These aspects have been investigated by employing CO as a surface probe molecule.

3.2. Surface Ni sites in samples treated in O_2

Infrared spectroscopy of CO adsorbed at low temperature (about 100 K) was adopted to investigate the different types of Ni surface sites present in the samples. In the experiments described below, care was taken to maintain the samples in oxidizing conditions during the whole activation step, in order to avoid Ni^{2+} reduction, which can occur according to literature [22-24]. In this respect it is worth noticing that on oxidized samples CO adsorption was carried out also at RT, but no appreciable adsorption bands could be observed. This is at variance with respect to the works by Hadjiivanov et al. on Ni-ZSM-5 samples [3, 14, 25] and with what recently reported by Martínez et al. who suggested a reducing effect of CO at RT on Ni^{2+} ions [22].

Figure 2 shows the spectra of CO adsorbed at 100 K on Comm-Ni zeolites as a function of CO coverage (θ_{CO}). Figure 3 is the same for NS-Ni samples. In all the cases, the infrared spectra at high CO coverage (θ_{max}) are dominated by three intense absorption bands at 2175, 2160 and 2138 cm^{-1},which have been previously assigned to CO adsorbed on Brønsted sites, silanols and CO condensed inside the zeolite's channels ('liquid-like'), respectively [5]. These bands, which are not related to Ni species, are labelled in the Figures as B, S and L, respectively. Moreover, a weak band is observed with different intensity on the four samples

at 2090 cm^{-1}. According to previous reports, this band could be related to relatively unstable adducts in which CO is interacting through the oxygen end or to a small contribution from the naturally less abundant $^{13}C^{16}O$ isotope [26, 27].

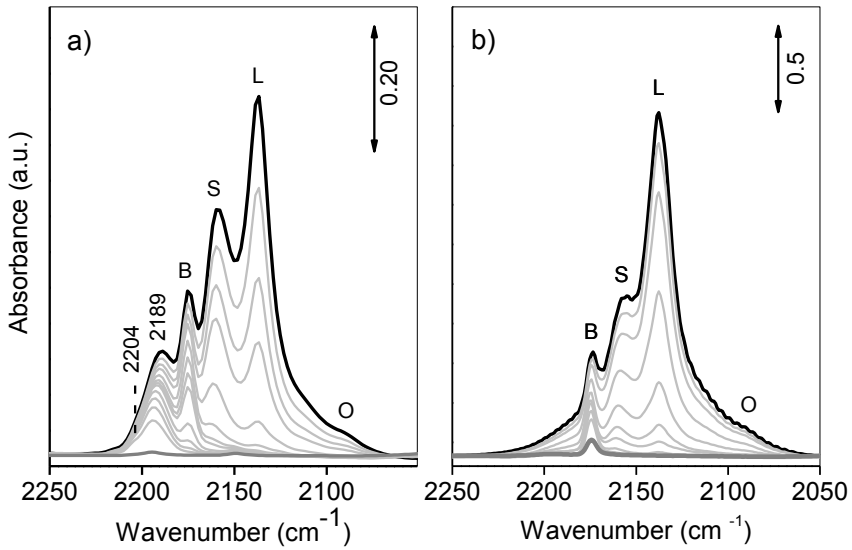

Figure 2. Low temperature infrared CO spectra measured on commercial oxidised samples: a) Comm-Ni/impr b) Comm-Ni/i.e. samples. Labels indicate band assignment: S) CO/Si-OH (silanols) adducts; B) CO/H^+ (Brønsted adducts); L) CO liquid-like (aspecific); O) O-bonded CO adducts or $^{13}C^{16}O$ isotope (see text).

The band at 2175 cm^{-1} has a larger relative intensity in the two commercial samples with respect to NS ones which is in agreement with the higher intensity of the Si(OH)Al band at 3613 cm^{-1} described above. Similarly, the different relative intensity of the bands at 2160 and 2175 cm^{-1} (CO adducts on silanols and Brønsted sites, respectively) in the ion exchanged and impregnated samples is strictly related to the observations in the ν(OH) region described in Section 3.1. These bands were the only ones observed on the parent Ni-free H-ZSM-5 materials.

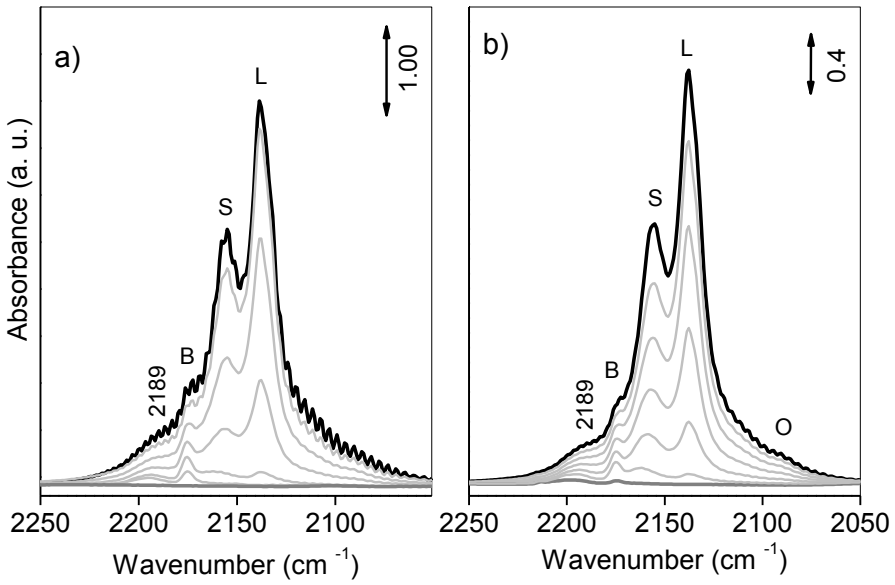

Figure 3. Low temperature infrared CO spectra measured on nano-sheet oxidised samples: a) NS-Ni/impr b) NS-Ni/i.e. samples. Labels indicate band assignment: S) CO/Si-OH (silanols) adducts; B) CO/H^+ (Brønsted adducts); L) CO liquid-like (aspecific); O) OC adducts or $^{13}C^{16}O$ isotope (see text).

Beside the bands described above, the main component observed on the Ni-containing samples (particularly on sample Comm-Ni/impr) is at 2189 cm^{-1} (value measured at θ_{max}), with an evident shoulder at 2204 cm^{-1}at low θ_{CO} (left panel of Figure 2). The former band is found to be coverage dependent, in that it gradually moves to higher frequency upon lowering θ_{CO} (maximum at 2194 cm^{-1} at θ_{min}).The band position is similar to that observed for CO adsorbed on Ni sites grafted on SiO_2 surface [3, 14, 28], suggesting that in sample Comm-Ni/impr most of Ni^{2+} atoms are incorporated into the zeolite structure by grafting. This is not surprising since the starting material showed a large amount of hydrogen-bonded defective Si-OH groups, while the high Si/Al ratio of the ZSM5 samples (Si/Al>50) does not favour

the ion exchange of a divalent ion as Ni^{2+}. In the other three samples bands in this region are very weak and overlapped to the high frequency range tail of the silanols/Brønsted CO adducts. However, interesting observations can be done by analysing a magnification of the spectra measured at low θ_{CO} (Figure 4).

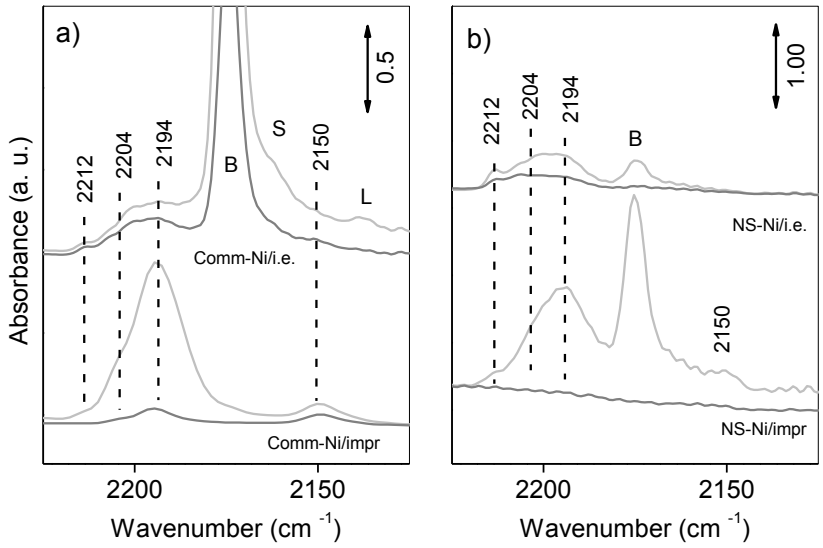

Figure 4. Magnification of the low temperature θ_{min} spectra measured on oxidized samples: a) commercial Ni/ZSM-5 and b) NS Ni/ZSM-5. See text and Figures 2 and 3 for labels.

In all samples very weak absorptions can be observed at 2212 and 2204 cm^{-1}, close to the band at 2194 cm^{-1} previously assigned to CO adducts on grafted Ni^{2+} ions (Figure 4). In the spectra of some of the samples (Comm-Ni/impr, Comm-Ni/i.e. and NS-Ni/impr) a very weak band is also observed at 2150 cm^{-1}. The band at 2212 $cm^{-1}$is quite typical of ion exchanged Ni-ZSM5 samples (usually with lower Si/Al ratio with respect to what reported in this study), and were assigned to mono-carbonyl Ni^{2+}-CO species formed on Ni^{2+} counter ions [3, 14]. The assignment of the band at 2204 cm^{-1} is more controversial, since it was explained as a

component of a $Ni^{2+}(CO)_2$ complex formed on different Ni^{2+}cationic sites [25] or to CO adducts on $[Ni\text{-}OH]^+$counterions [14], The former assignment is dubious in the present case, since it is mainly observed at low θ_{CO}, at variance with what usually found with dicarbonyls. Finally, bands at 2150 cm^{-1} (shifting at lower frequency by increasing θ_{CO}) were observed upon CO adsorption on low surface area NiO particles [29],

By comparing the normalized spectra of CO adsorbed on the different Ni-containing samples at low θ_{CO} (Figure 4) the following observations can be done:

1) the relative intensity of the bands at 2212 and 2204 $cm^{-1}$with respect to the band at 2194 $cm^{-1}$is higher in ion-exchanged samples than in impregnated ones, indicating a larger amount of Ni^{2+} counterions when Ni is inserted via ion-exchange method.

2) The component at 2150 cm^{-1} is more evident on commercial samples (left panel of Figure 4) and is totally absent in sample NS-Ni/i.e (top part of right panel). This suggests the presence of NiO aggregates/particles, probably dispersed on the external surface of the zeolites, which are favoured by impregnation on Si-OH rich samples (commercial ones).

Finally, it is worth noticing that the overall intensity of the bands related to surface Ni species (particularly the band at 2194 cm^{-1}) is much more intense in sample Comm-Ni/impr, irrespective of the fact that this sample has the same Ni loading than NS-Ni/impr (2 wt%, see Table 1). This observation indicates that a larger fraction of Ni ions are exposed in the commercial sample, with respect to NS-Ni/impr, *i.e.* the Ni dispersion is higher. This could be related to the larger abundance of defective Si-OH groups, favouring the grafting of a high amount of dispersed Ni species.

3.2. Self-reduction, in samples activated in vacuum

As mentioned above, many authors reported in the literature about the reduction of Ni^{2+} to Ni^{+} as a result of activation in CO at relatively high temperature,[11,12,22] or even upon contact with ethylene.[30] Moreover, recent reports pointed to the possibility to obtain Ni^{+} formation upon CO adsorption at RT on Ni^{2+} containing zeolites, opening some questions on the results obtained on these experimental conditions.[22] In the present study, the possibility to obtain the so-called 'self-reduction' of Ni^{2+} to Ni^{+} was studied on the samples activated in vacuum conditions. As observed on the samples treated in O_2 (see above), CO adsorption at RT on samples activated in vacuum did not result in the formation of stable CO adducts in appreciable concentration. This suggests that the reducing ability of CO, testified by Martínez et al. on Ni-H-Beta catalysts with Si/Al =12 and Ni loading in the range 1.0-2.5 wt % [22], is not efficient on the samples reported in this work. This in turns implies that the reducibility of Ni species stabilized in zeolite frameworks strongly depends upon many factors, such as Si/Al ratio, Ni loading and samples preparation, as already pointed out by Penkova et al. [31].

To shed more light on this aspect, CO adsorption at LT was carried out on the four Ni-ZSM-5 samples after activation in vacuum at 400 °C. Similarly to what seen on the oxidized samples, at high θ_{CO} the CO spectra are dominated by the B, S and L bands (see Figures 2 and 3). Thus, information about Ni speciation can be obtained by analysis of the spectra obtained at low θ_{CO}. The spectra obtained on samples Comm-Ni/impr and NS-Ni/i.e. show distinct differences with respect to what seen in the oxidized form, as reported in Figure 5. Interestingly, these samples are also the only two where a significant difference was observed in the ν(OH) region with respect to the parent materials (compare curves a and b in left part of Figure 1 and curves a and c in the corresponding right hand panel). The spectra obtained

on the other two samples (Comm-Ni/i.e. and NS-Ni/impr) do now show appreciable differences with respect to the oxidized ones and are thus not reported.

The spectra obtained at LT on samples Comm-Ni/impr and NS-Ni/i.e (Figure 5a,b) are similar, with some differences in the relative intensity of the bands. First, bands related to $Ni^{2+}(CO)$ adducts formed on Ni^{2+}counterions are still present in both samples (band at 2212 cm^{-1}), while the band at 2194 cm^{-1}, previously assigned to CO on grafted Ni^{2+}only forms at higher θ_{CO}. In the range typical for Ni^{2+} complexes other two bands are observed at 2222 and 2205 cm^{-1}. Based on literature reports, the former can be assigned to a $Ni^{2+}(CO)$ complex formed on second type of Ni^{+} counterions (labelled with a star in Figure 5) [3], while the latter is related to the formation of counterionic $Ni^{2+}(CO)_2$ complexes [25]. Moreover, bands at lower frequency can be easily assigned to CO adducts on Ni^{+} and on Ni^{0} surface sites. More in detail, the band at 2109 cm^{-1} is assigned to a $Ni^{+}(CO)$ complex, evolving in $Ni^{+}(CO)_2$ ones upon increase in θ_{CO} (bands at 2137 and 2093 cm^{-1}). These species are typical of reduced Ni-zeolites and were assigned to mono- and dicarbonyls on Ni^{+} counterions. Finally, the band at 2045 cm^{-1} can be explained with the formation of $Ni^{0}(CO)_4$ species, and thus testifies of the formation of metal Ni^{0} particles [32, 33]. This band is more intense on sample Comm-Ni/impr. These results indicate that a small, but not negligible fraction of Ni^{2+} species in the two samples are reduced to Ni^{+} (which are stabilized as counterions by the negative charges of the framework) and to Ni^{0} particles, which can be located in the zeolite channels and on the zeolite external surface. Moreover, a higher fraction of Ni^{2+} ions are stabilized as counterions with respect to what observed on the oxidized samples, where grafted Ni^{2+} species where the dominant ones, implying a redistribution of the metal species during

activation. In this respect, it is important to underline the fact that in this work no quantitative considerations are made with respect to the amount of Ni^{2+}, Ni^{+} or Ni^{0} species present in the different samples. Góra-Marek et al. reported interesting infrared results where Ni^{2+} and Ni^{+} ions in ZSM-5 samples were quantified based on the calculation of the extinction coefficients of the corresponding CO bands (REF). Namely, they measured values of ε equal to 0.143 ± 0.003 and 1.104 ± 0.018 $cm^2/\mu mol$ for Ni^{2+}(CO) (band at 2212 cm^{-1}) and Ni^{+}(CO) (band at 2109 cm^{-1}) adducts. This supports our evidence that the amount of Ni^{2+} 'self-reduced' to Ni^{+} is very small. However, no further quantitative considerations can be made, due the complexity of the spectra which is related to the presence of NiO and Ni^{0} aggregates/particles.

To further investigate the mechanisms related to these redox and mobility phenomena, attention was devoted to the analysis of the zeolite spectra of the two samples activated in different conditions.

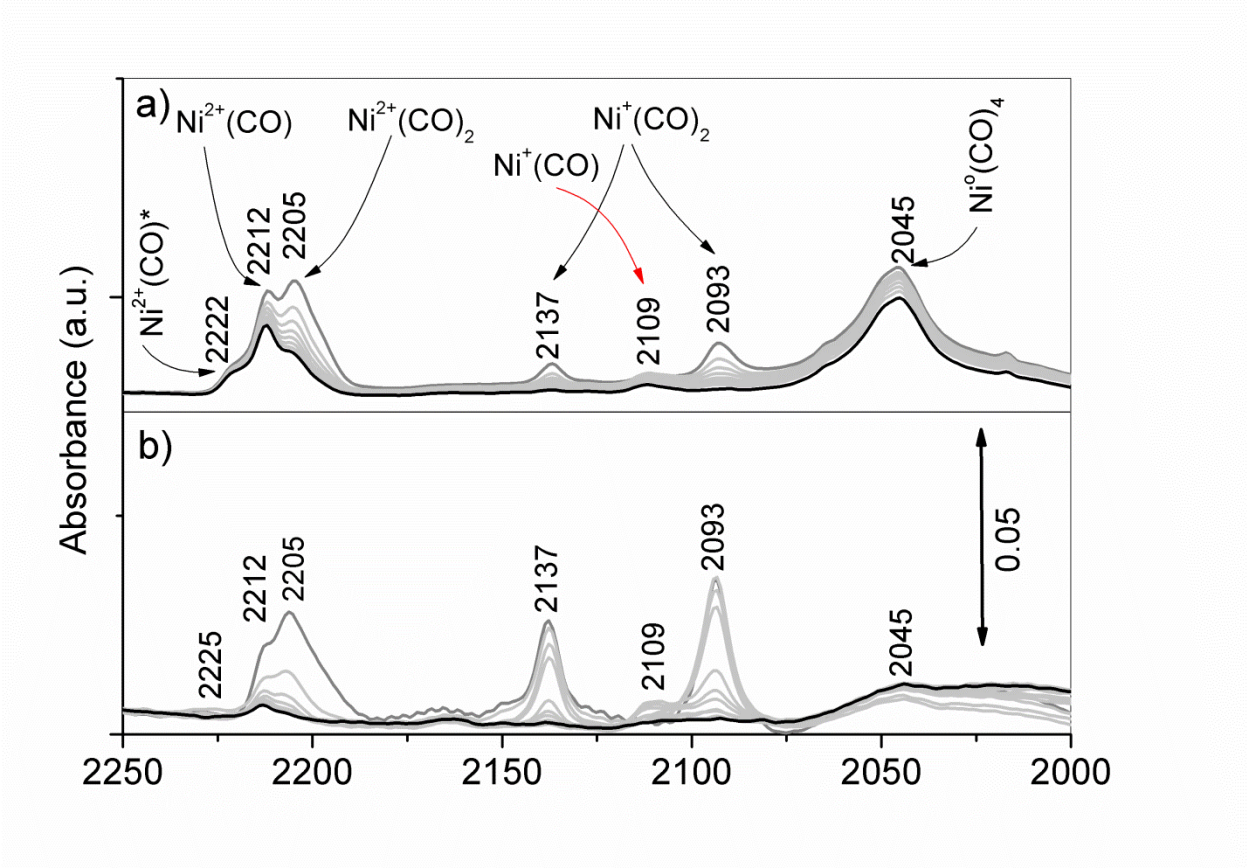

Figure5. CO adsorption at 110 K on samples activated at 400 °C in vacuum on Comm-Ni/impr (a) and NS-Ni/i.e. (b). See text for band assignment.

Figure 6 reports the spectra of samples Comm-Ni/ impr and NS-Ni/i.e. (Figure 6a and b, respectively) after activation in O_2 (black curve) and in vacuum (grey curves). Attention is paid to the two more informative regions, that is the ν(OH) one (3800-3250 cm^{-1}) and the so-called 'window region' (950-850 cm^{-1}). The ν(OH) spectra of oxidized samples have been already discussed in section 3.1 and are only briefly summarized hereafter. Shortly, both samples show the typical modes of isolated silanols (3740/3744 cm^{-1}) and of Si(OH)Al Brønsted sites (3613 cm^{-1}), although if the latter is very weak on sample NS-Ni/i.e. Moreover,

Comm-Ni/ impr sample shows a band at 3658 cm^{-1}, which was tentatively assigned to a [Ni-OH]$^+$ counterion, and a broad absorption around 3500 cm^{-1}, ascribed to hydroxyl nests. On the contrary the spectrum of NS-Ni/i.e. (nanosheet morphology) only shows a tail down to 3250 cm^{-1} with a weak bands at 3670 cm^{-1} (extra-framework Al-OH).

When the sample is activated in vacuum, the ν_{OH} spectrum of sample Comm-Ni/ impr are highly affected, in that the overall intensity decreases in the whole region. This is less evident in sample NS-Ni/i.e., even if small changes are observed in the intensity of the bands related to Brønsted sites and extra-framework Al-OH groups. In both samples changes are observed in the 'window region', where a band at approximately 894 cm^{-1} grows, more evidently in sample NS-Ni/i.e (this band has a shoulder in the case of NS-Ni/i.e sample). Similar bands were observed on metal ion exchanged zeolites and explained with the perturbation of T-O-T modes by the presence of the counterions (see for instance the work by Broclawik et al. and references therein [REF]). However, this band is also present on the metal-free nanosheet H-ZSM-5 sample, and was assigned to strained Si-O-Si bridges [5]. This is particularly strong in nanosheet samples, due to the higher amount of surface T atoms, implying a higher number of defects. The shoulder can also be assigned to the strained T-O-T with different distortion value or different cationic sites. These changes suggest that the surface of both samples changes in terms of OH populations, which are consumed in vacuum conditions, resulting in a higher concentration of defects with respect to what obtained in the presence of oxygen.

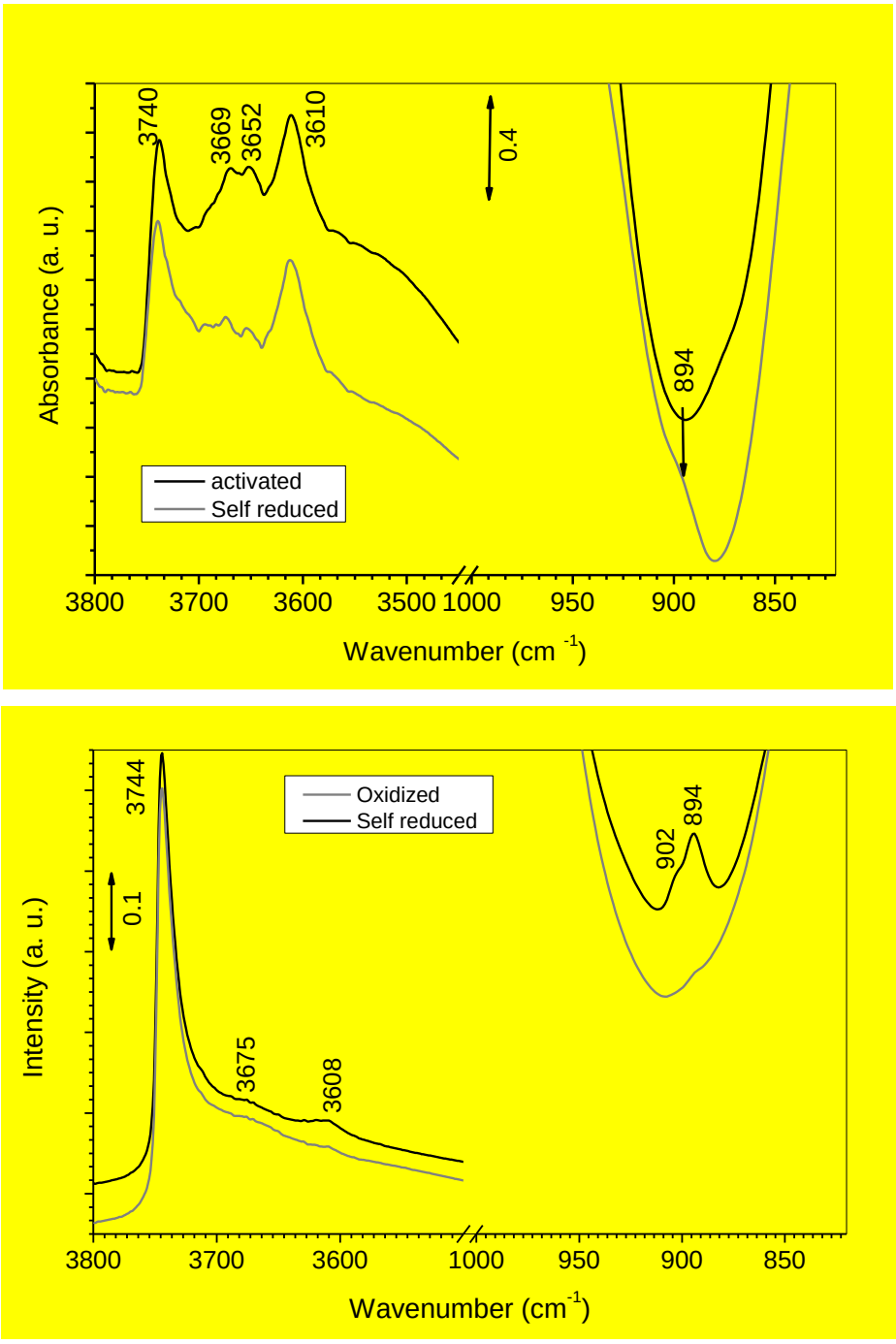

Figure 6. Comparison of infrared spectra of samples activated in oxygen and vacuum conditions (black and grey curves, respectively) on samples Comm-Ni/impr (top) and NS-Ni/i.e. (bottom)

3.3. Summary of main findings

The main information obtained from the detailed spectroscopic analysis described above can be summarized as follows.

First, this work shows how the nanosheet morphology favours ion exchange, even at a relatively high Si/Al ratio (around 50). On the contrary, grafted Ni^{2+} ions are in relatively large amount on the commercial sample prepared. The presence of $[Ni\text{-}OH]^{+}$ counterions, in analogy with what observed on Cu-exchanged zeolites, cannot be proven neither excluded with certainty [17].

When impregnation method is employed in both micron-sized and nanosheet zeolites, NiO particles are formed, as testified by a band at 2150 cm^{-1} due to CO adducts. However, in the nanosheet sample prepared by impregnation, the overall intensity of CO bands related to Ni sites on the surface of NiO particles is much lower with respect to the commercial sample with the same Ni loading. This suggests that in NS-Ni/impr sample bigger NiO particles are formed, which result in lower Ni dispersion.

This is also confirmed by experiments carried out on the samples activated in vacuum. In this case, a fraction of Ni^{2+} is reduced to Ni^{+} and Ni^{0} only on the commercial sample prepared by impregnation (Comm-Ni/impr) and on the ion exchanged nanosheet one (NS-Ni/i.e.), that is on the two samples with higher Ni dispersion. The formation of Ni^{0} particles (testified by the CO band at 2045 cm^{-1}, assigned to $Ni^{0}(CO)_4$ complexes) is more important on the former, suggesting that these are formed by oxygen depletion from small NiO particles, similarly to redox mechanisms observed on NiO supported on oxides [32, 33]. The fact that the same phenomenon is not observed on the nanosheet sample with same Ni loading

(NS-Ni/impr) is in agreement with the presence of relatively bigger and less reactive NiO particles.

4. Conclusions

The results discussed above can be analysed to shed light on the different insertion mechanism of Ni ions in zeolites with different morphology and high Si/Al ratio. First, the higher efficacy of the ion exchange process in the samples with nanosheet morphology can be explained by the presence of a high amount of surface T sites, as proposed elsewhere [5]. This means that a large fraction of Ni^{2+} ions can be stabilized without further reaction with surface Si-OH groups. On the contrary, in samples with micron sized morphology and a relatively high amount of Si-OH groups, ion exchange and grafting processes are in competition and the efficiency of ion exchange is lower.

On the other hand, the presence of Si-OH rich surfaces on the external surface of the zeolites and/or inside the pores favour the stabilization of relatively small NiO particles. These particles are highly reactive, in that Ni^{2+} sites in NiO are easily reduced to Ni^{+} and Ni^{0} by simple activation in vacuo, and can migrate to counterionic positions. On the contrary, in the Si-OH poor nanosheet sample, larger NiO particles are formed, which show lower reactivity and mobility of Ni species.

These observations confirm the important role of surface Si-OH groups (particularly those present in hydroxyl rich regions) in stabilizing metal ions in zeolites and tuning their properties (oxidation state and nuclearity). These reactive surfaces sites (which can form strained Si-O-Si bridges as a consequence of dehydration) competes with negatively charged

SiOAl groups for the stabilization of metal ions, and infer to them a higher mobility and flexibility with respect to counterions.

These results can have a general interest in the field of heterogeneous catalysis, since they give some hints about the insertion mechanism of bivalent ions in zeolites, which show a relatively high mobility among surface sites available for their stabilization (negative framework charges in correspondence of Al T sites and hydroxyl nests) and relatively easy redox ability, which is probably mediated by surface OH groups. This could explain the large heterogeneity of situations described in the literature about characterization of Ni-zeolites. Finally, it is likely to infer that the same mobility is observed in the presence of reactants, so that a precise description of an active sites in catalysis can become a difficult challenge.

Acknowledgment

We would like to thank Prof. Unni Olsbye, Mr. Henry Reynald and Dr. Rasmus Yding Brogaard, University of Oslo for samples preparation and for fruitful discussion.

References

[1] M. Trombettaa, G. Buscaa, S. Rossinib, V. Piccolib, U. Cornarob, FT-IR Studies on Light Olefin Skeletal Isomerization Catalysis: II. The Interaction of C4 Olefins and Alcohols with HZSM5 Zeolite, Journal of catalysis, 168 (1997) 349-363.
[2] G. Spoto, S. Bordiga, G. Ricchiardi, D. Scarano, A. Zecchina, E. Borello, IR study of ethene and propene oligomerization on H-ZSM-5: hydrogen-bonded precursor formation, initiation and propagation mechanisms and structure of the entrapped oligomers, J. Chem. Soc. Faraday Trans., 90 (1994) 2827-2835.

[3] M. Mihaylov, K. Hadjiivanov, FTIR Study of CO and NO Adsorption and Coadsorption on Ni-ZSM-5 and Ni/SiO_2, Langmuir, 18 (2002) 4376-4383.
[4] P. Castaño, G. Elordi, M. Olazar, A.T. Aguayo, B. Pawelec, J. Bilbao, Insights into the coke deposited on HZSM-5, Hβ and HY zeolites during the cracking of polyethylene, Applied Catalysis B: Environmental, 104 (2011) 91-100.
[5] B.-T.L. Bleken, L. Mino, F. Giordanino, P. Beato, S. Svelle, K.P. Lillerud, S. Bordiga, Probing the surface of nanosheet H-ZSM-5 with FTIR spectroscopy, Phys. Chem. Chem. Phys., 15 (2013) 13363-13370.
[6] M. Choi, K. Na, J. Kim, Y. Sakamoto, O. Terasaki, R. Ryoo, Stable single-unit-cell nanosheets of zeolite MFI as active and long-lived catalysts, Nature , , 461 (2009) 246-249.
[7] M.C. K Na, W. Park, Y. Sakamoto, O. Terasaki, R. Ryoo, Pillared MFI zeolite nanosheets of a single-unit-cell thickness, Journal of the American Chemical Society, 132 (2010) 4169-4177.
[8] J. Čejka, G. Centi, J. Perez-Pariente, W.J. Roth, Zeolite-based materials for novel catalytic applications: Opportunities, perspectives and open problems, Catalysis Today, 179 (2012) 2-15.
[9] Y. Li, W.K. Hall, Stoichiometric catalytic decomposition of nitric oxide over copper-exchanged zeolite (CuZSM-5) catalysts, J. Phys. Chem., 94 (1990) 6145-6148.
[10] J. Tang, T. Zhang, L. Ma, L. Li, J. Zhao, M. Zheng, L. Lin, Microwave discharge-assisted NO reduction by CH_4 over Co/HZSM-5 and Ni/HZSM-5 under O_2 excess, Catalysis Letters, 73 (2001) 193-197.
[11] A.I. Serykh, M.D. Amiridis, Formation and Thermal Stability of Ni^+ Cationic Sites in Ni-ZSM-5, J. Phys. Chem. C, 111 (2007) 17020-17024.
[12] P. Pietrzyk, T. Mazur, K. Podolska-Serafin, M. Chiesa, Z. Sojka, Intimate Binding Mechanism and Structure of Trigonal Nickel(I) Monocarbonyl Adducts in ZSM-5 Zeolite—Spectroscopic Continuous Wave EPR, HYSCORE, and IR Studies Refined with DFT Quantification of Disentangled Electron and Spin Density Redistributions along σ and π Channels, Journal of the American Chemical Society, 135 (2013) 15467-15478.
[13] P. Pietrzyk, K. Podolska, Z. Sojka, Role of NOδ+ Intermediates in NO Reduction with Propene over NiZSM-5 Zeolite Revealed by EPR and IR Spectroscopic Investigations and DFT Modeling, The Journal of Physical Chemistry C, 115 (2011) 13008-13015.
[14] K. Hadjiivanov, H. Knozinger, M. Mihaylov, FTIR Study of CO Adsorption on Ni-ZSM-5, J. Phys. Chem. B, 106 (2002) 2618-2624.
[15] K. Na, W. Park, Y. Seo, R. Ryoo, Disordered Assembly of MFI Zeolite Nanosheets with a Large Volume of Intersheet Mesopores, Chemistry of Materials, 23 (2011) 1273-1279.
[16] S. Svelle, L. Sommer, K. Barbera, P.N.R. Vennestrøm, U. Olsbye, K.P. Lillerud, S. Bordiga, Y.-H. Pan, P. Beato, How defects and crystal morphology control the effects of desilication, Catalysis Today, 168 (2011) 38-47.
[17] F. Giordanino, P.N. Vennestrøm, L.F. Lundegaard, F.N. Stappen, S. Mossin, P. Beato, S. Bordiga, C. Lamberti, Characterization of Cu-exchanged SSZ-13: a comparative FTIR, UV-Vis, and EPR study with Cu-ZSM-5 and Cu-β with similar Si/Al and Cu/Al ratios, Dalton Transactions, 42 (2013) 12741-12761.

[18] M. Che, Z.X. Cheng, C. Louis, Nucleation and Particle Growth Processes Involved in the Preparation of Silica-Supported Nickel Materials by a Two-Step Procedure, J. Am. Chem. Soc., 117 (1995) 2008-2018.
[19] J.-F. Lambert, M. Hoogland, M. Che, Control of the Ni^{II}/Surface Interaction in the First Steps of Supported Catalyst Preparation: The Interfacial Coordination Chemistry of $[Ni(en)_2(H_2O)_2]^{2+}$Control of the Ni^{II}/Surface Interaction in the First Steps of Supported Catalyst Preparation: The Interfacial Coordination Chemistry of $[Ni(en)_2(H_2O)_2]^{2+}$, J. Phys. Chem. B 101 (1997) 10347-10355.
[20] G. Martra, S. Coluccia, M. Che, L. Manceron, M. Kermarec, D. Costa, Ni and CO Used as Probes of the Amorphous Silica Surface: IR and Theoretical Studies of Dicarbonyl NiII Complexes†, J. Phys. Chem. B, 107 (2003) 6096-6104.
[21] S.F. Ruzankin, I.V. Shveigert, G.M. Zhidomirov, Nest Defect as the Site of Stabilization of Transition Element Ions Implanted in High-Silica Zeolites. Cluster Calculation of Fe(II) and Fe(III) Ions Entrapped by the Zeolite Matrix, Journal of Structural Chemistry, 43 (2002) 229-233.
[22] A. Martínez, M.A. Arribas, P. Concepción, S. Moussa, New bifunctional Ni-H-Beta catalysts for the heterogeneous oligomerization of ethylene, Applied Catalysis A: General, 467 (2013) 509-518.
[23] M. Hartmann, A. Pöppl, L. Kevan, Ethylene Dimerization and Butene Isomerization in Nickel-Containing MCM-41 and AlMCM-41 Mesoporous Molecular Sieves: An Electron Spin Resonance and Gas Chromatography Study, The Journal of Physical Chemistry, 100 (1996) 9906-9910.
[24] M. Lallemand, A. Finiels, F. Fajula, V. Hulea, Nature of the Active Sites in Ethylene Oligomerization Catalyzed by Ni-Containing Molecular Sieves: Chemical and IR Spectral Investigation, The Journal of Physical Chemistry C, 113 (2009) 20360-20364.
[25] H.A. Aleksandrov, V.R. Zdravkova, M.Y. Mihaylov, P.S. Petkov, G.N. Vayssilov, K.I. Hadjiivanov, Precise Identification of the Infrared Bands of the Polycarbonyl Complexes on Ni−MOR Zeolite by $^{12}C^{16}O$–$^{13}C^{18}O$ Coadsorption and Computational Modeling, J. Phys. Chem. C, 116 (2012) 22823−22831.
[26] P. Ugliengo, E. Garrone, A.M. Ferrari, A. Zecchina, C. Otero Areán, Quantum Chemical Calculations and Experimental Evidence for O-Bonding of Carbon Monoxide to Alkali Metal Cations in Zeolites, The Journal of Physical Chemistry B, 103 (1999) 4839-4846.
[27] L. Mino, G. Spoto, S. Bordiga, A. Zecchina, Particles Morphology and Surface Properties As Investigated by HRTEM, FTIR, and Periodic DFT Calculations: From Pyrogenic TiO2 (P25) to Nanoanatase, The Journal of Physical Chemistry C, 116 (2012) 17008-17018.
[28] K. Hadjiivanov, M. Mihaylov, D. Klissurski, P. Stefanov, N. Abadjieva, E. Vassileva, L. Mintchev, Characterization of Ni/SiO_2 Catalysts Prepared by Successive Deposition and Reduction of Ni^{2+} Ions, J. Catal., 185 (1999) 314-326.
[29] A. Zecchina, D. Scarano, S. Bordiga, G. Spoto, C. Lamberti, Surface structures of oxides and halides and their relationships to catalytic properties, Advances in Catalysis, 46 (2001) 265-397.
[30] T. Cai, Studies of a new alkene oligomerization catalyst derived from nickel sulfate, Catalysis Today, 51 (1999) 153-160.

[31] A. Penkova, S. Dzwigaj, R. Kefirov, K. Hadjiivanov, M. Che, Effect of the Preparation Method on the State of Nickel Ions in BEA Zeolites. A Study by Fourier Transform Infrared Spectroscopy of Adsorbed CO and NO, Temperature-Programmed Reduction, and X-Ray Diffraction, The Journal of Physical Chemistry C, 111 (2007) 8623-8631.
[32] S. Gopalakrishnan, M.G. Faga, I. Miletto, S. Coluccia, G. Caputo, S. Sau, A. Giaconia, G. Berlier, Unravelling the structure and reactivity of supported Ni particles in Ni-CeZrO2 catalysts, Applied Catalysis B: Environmental, 138–139 (2013) 353-361.
[33] S. Morandi, M. Manzoli, F. Prinetto, G. Ghiotti, C. Gérardin, D. Kostadinova, D. Tichit, Supported Ni catalysts prepared by intercalation of Layered Double Hydroxides: Investigation of acid–base properties and nature of Ni phases, Microporous and Mesoporous Materials, 147 (2012) 178-187.